
**Mechanisms of Signal Transduction:
Solution Structure of the C-terminal
Domain of the Ciliary Neurotrophic Factor
(CNTF) Receptor and Ligand Free
Associations among Components of the
CNTF Receptor Complex**

David Man, Wei He, Kong Hung Sze, Ke
Gong, David K. Smith, Guang Zhu and Nancy
Y. Ip

J. Biol. Chem. 2003, 278:23285-23294.

doi: 10.1074/jbc.M301976200 originally published online April 21, 2003

Access the most updated version of this article at doi: [10.1074/jbc.M301976200](https://doi.org/10.1074/jbc.M301976200)

Find articles, minireviews, Reflections and Classics on similar topics on the [JBC Affinity Sites](https://www.jbc.org/).

Alerts:

- [When this article is cited](#)
- [When a correction for this article is posted](#)

[Click here](#) to choose from all of JBC's e-mail alerts

This article cites 47 references, 13 of which can be accessed free at
<http://www.jbc.org/content/278/26/23285.full.html#ref-list-1>

Solution Structure of the C-terminal Domain of the Ciliary Neurotrophic Factor (CNTF) Receptor and Ligand Free Associations among Components of the CNTF Receptor Complex*

Received for publication, February 25, 2003, and in revised form, April 16, 2003
Published, JBC Papers in Press, April 21, 2003, DOI 10.1074/jbc.M301976200

David Man‡, Wei He‡, Kong Hung Sze, Ke Gong, David K. Smith§, Guang Zhu¶, and Nancy Y. Ip||

From the Department of Biochemistry and Biotechnology Research Institute, Hong Kong University of Science and Technology, Clear Water Bay, Hong Kong and the §Department of Biochemistry, University of Hong Kong, Hong Kong, China

The functional receptor complex of ciliary neurotrophic factor (CNTF), a member of the gp130 family of cytokines, is composed of CNTF, the CNTF receptor α (CNTFR), gp130, and the leukemia inhibitory factor receptor (LIFR). However, the nature of the receptor-mediated interactions in this complex has not yet been resolved. To address this issue we have determined the solution structure of the C-terminal or BC domain of CNTFR and studied the interactions of CNTFR with LIFR and gp130. We reported previously that the membrane distal cytokine-binding domain (CBD1) of LIFR could interact *in vitro* with soluble CNTFR (sCNTFR) in the absence of CNTF. Here we show that the CBD of human gp130 can also bind *in vitro* to sCNTFR in the absence of CNTF. In addition, the gp130 CBD could compete with the LIFR CBD1 for the binding of sCNTFR. Substitution of residues in the gp130 CBD, the LIFR CBD1, and the CNTFR BC domain that are expected to be involved in receptor-receptor interactions significantly reduced their interactions. An NMR chemical shift perturbation study of the interaction between the BC domains of CNTFR and gp130 further mapped the interaction surface. These data suggest that both the gp130 CBD and the LIFR CBD1 interact with CNTFR in a similar way and provide insights into the nature of the CNTF receptor complex.

Ciliary neurotrophic factor (CNTF)¹ belongs to the gp130 family of cytokines. This family also includes leukemia inhibi-

* This work was supported in part by the Research Grants Council of Hong Kong HKUST6124/02M, HKUST6127/99M, and HKUST6199/99M and the Hong Kong Jockey Club. The costs of publication of this article were defrayed in part by the payment of page charges. This article must therefore be hereby marked "advertisement" in accordance with 18 U.S.C. Section 1734 solely to indicate this fact.

The atomic coordinates and structure factors (code 1UC6) have been deposited in the Protein Data Bank, Research Collaboratory for Structural Bioinformatics, Rutgers University, New Brunswick, NJ (<http://www.rcsb.org/>).

‡ These authors contributed equally to this work.

¶ To whom correspondence may be addressed. E-mail: gzhu@ust.hk.
|| Recipient of a Croucher Foundation Senior Research Fellowship. To whom correspondence may be addressed: Dept. of Biochemistry, Hong Kong University of Science and Technology, Clear Water Bay, Hong Kong, China. Tel.: 852-2358-7289; Fax: 852-2358-2765; E-mail: BOIP@UST.HK.

¹ The abbreviations used are: CNTF, ciliary neurotrophic factor; CNTFR, CNTF receptor; sCNTFR, soluble CNTFR; r.m.s.d., root mean square deviation; LIFR, leukemia inhibitory factor receptor; IL, interleukin; CBD, cytokine binding domain; NOE, nuclear Overhauser effect; NOESY, nuclear Overhauser effect spectroscopy; GST, glutathione

tory factor, interleukin (IL)-6, IL-11, oncostatin M, cardiotrophin-1, and the newly identified cardiotrophin-like cytokine (1–3). Among its many functions, CNTF enhances the survival of neuronal cells (4) and has been investigated as a therapeutic agent for motor neuron disease (5). Recently, it has been shown to have a promising role in the treatment of obesity and diabetes (6) and recognized as a major protective factor in demyelinating central nervous system disease (7). To exert its biological functions, CNTF first binds its non-signaling, specific receptor, CNTFR, which has been shown to be required for motor neuron development (8). Signaling through the JAK/signal transducers and activators of transcription pathway follows the recruitment of gp130 and the leukemia inhibitory factor receptor (LIFR) (9, 10).

These receptors are members of the class I hematopoietin receptor family, which is characterized by a cytokine binding domain (CBD) formed from two fibronectin type III (FnIII) modules linked by a proline-rich sequence (11). Class I hematopoietin receptors contain four conserved cysteine residues that form inter-strand disulfide bonds in the N-terminal FnIII (BN) module of the CBD and a conserved WSXWS sequence in the C-terminal FnIII (BC) module. CNTFR, gp130, and LIFR have a related modular structure in their extracellular regions (Fig. 1). CNTFR contains an N-terminal immunoglobulin (Ig)-like module and a CBD; gp130 has the same structure but with three membrane-proximal FnIII modules, and LIFR is the same as gp130 but with an additional N-terminal CBD. Of these receptors, only the tertiary structures of the gp130 BC module, the gp130 CBD and the gp130 Ig-CBD domains, have been determined (12–14). The BN and BC modules of the CBD each consist of seven anti-parallel β -strands, which form two β -sheets. Recently, the complete NMR assignments of the BC module of CNTFR have been reported (15).

In vitro, CNTF has been shown to form a hexameric receptor complex composed of two molecules each of CNTF and CNTFR and one molecule each of gp130 and LIFR (16). The hexameric nature of the related IL-6 signaling complex (17, 18) and the proposal that the IL-6 signaling complex is formed by two trimers of IL-6, IL-6R and gp130 linked by the gp130 Ig-like domain (19, 20), have been verified recently by crystallographic and biochemical studies (14, 21). Although the crystal structure of CNTF has been solved, revealing a four helix bundle and giving the location of the three sites, which are responsible for the binding of CNTFR, gp130, and LIFR (22, 23), the precise

S-transferase; FnIII, fibronectin type III; ELISA, enzyme-linked immunosorbent assay; PBS, phosphate-buffered saline; BSA, bovine serum albumin; IPTG, isopropyl-1-thio- β -D-galactopyranoside.

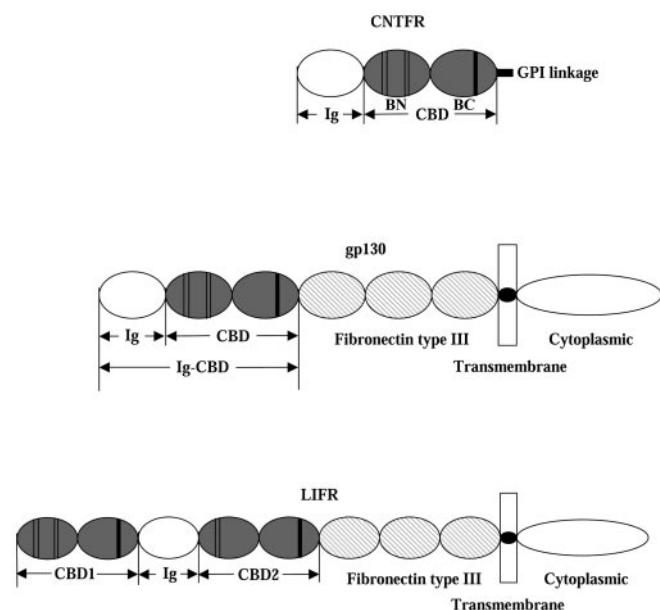


FIG. 1. Schematic representations of the modular structure of CNTFR, gp130, and LIFR. The receptor modules referred to in this study are indicated on the diagrams of the molecules. The BN and the BC domains, which together make up the CBD, contain, respectively, the two conserved disulfide bridges (thin lines) and the WSXWS motif (black bar) that are characteristic of these molecules.

nature of the protein-protein interactions in the CNTF receptor complex remains elusive. In particular, little is known about which domains of the receptors are involved in the interactions in the complex and the nature of the receptor-receptor interactions in the hexameric complex. As the CNTF receptor complex is asymmetric, containing one molecule each of gp130 and LIFR instead of two gp130 molecules as in the IL-6 receptor complex, a tetrameric, rather than hexameric, signaling complex for CNTF is still supported (24, 25).

Here we determine the solution structure of the CNTFR BC domain, the module likely to be involved in receptor-receptor interactions, and we investigate some of the receptor-receptor interactions in the CNTF complex and examine the possibility of ligand free association of receptor molecules. We reported recently (26) that the LIFR CBD1 could interact with soluble CNTFR *in vitro* in the absence of CNTF. It was found here that the gp130 CBD could also bind to soluble CNTFR *in vitro* in the absence of CNTF and compete with the LIFR CBD1 for binding to CNTFR. Residues in the B strand of the BC module of the gp130 CBD and in the putatively similar region of the LIFR CBD1 were shown to be important for the ligand free interaction of gp130 and LIFR with CNTFR. A mutation study of the BC domain of CNTFR also revealed residues important for the interaction with gp130, and NMR methods were used to further map these surfaces.

EXPERIMENTAL PROCEDURES

Expression Vectors for the Polyhistidine-tagged and Glutathione S-transferase Fusion Peptides—cDNA templates coding for full-length human CNTFR and rat CNTF were reverse transcriptase-PCR-amplified from mRNAs of NT-2 human embryonal carcinoma cells (Stratagene) and rat pheochromocytoma PC12 cells, respectively. Human gp130 and LIFR cDNA templates were reverse transcriptase-PCR-amplified from mRNA of SH-SY5Y human neuroblastoma cells. DNA sequencing was performed using an ABI PRISM 310 Genetic Analyzer autosequencer (PerkinElmer Life Sciences). DNA sequences were confirmed with the sequences in the GenBank™ data base. For NMR studies the BC domains of CNTFR (residues 202–305) and of gp130 (residues 219–325) were also amplified by PCR. The bacterial expression vector for His tag proteins was based on a modified pET-14b plasmid (Novagen) as described previously (26). The His-tagged sC-

NTFR construct was also labeled with a C-terminal c-Myc epitope. The bacterial expression vector for GST fusion proteins was pGEX 6-p-1 (Amersham Biosciences). For the expression of GST fusion proteins, a *Bam*HI site was introduced in the 5' sense primers, and a *Not*I or *Eco*RI (for peptides for NMR studies) site was introduced in the 3' antisense primers. After amplification, the PCR products were digested with *Bam*HI and *Not*I or *Eco*RI restriction enzymes and ligated into the pGEX 6-p-1 vector.

Protein Expression, Purification, and Refolding—*Escherichia coli* bacteria (strain BL21-DE3) were transformed with expression vectors pET-14b and pGEX-6-p-1 containing cDNAs for various peptides. Transformed bacteria were grown to an A_{600} of ~0.2 at 37 °C and induced by 1 mM IPTG (isopropyl-1-thio- β -D-galactopyranoside) for 4 h. Uniformly, 15 N and 15 N/ 13 C-labeled CNTFR BC domain peptides were prepared by growing the bacteria in M9 minimal medium using 15 NH₄Cl (1 g/liter) as the sole nitrogen source or 15 NH₄Cl (1 g/liter) and 13 C₆-labeled glucose (1 g/liter) as the sole nitrogen and carbon source, respectively. For the purification of His-tagged proteins, inclusion bodies were denatured in 8 M urea, pH 8.0. After binding to a nickel-nitrilotriacetic acid column (Qiagen), His-tagged peptides were eluted by 8 M urea, pH 4.5. Refolding of sCNTFR was as described previously (27), and refolding of other proteins was achieved by dialysis against refolding buffer (10 mM Tris, pH 8.0, 1 mM reduced glutathione, 0.1 mM oxidized glutathione, 36 h). Refolded proteins were loaded on a Q-Sepharose High Performance column (Amersham Biosciences) and eluted with a salt gradient using an Akta explorer 100 fast protein liquid chromatography purification system (Amersham Biosciences). For the purification of GST fusion proteins, supernatant of bacterial lysate after sonication was loaded on a glutathione-conjugated Sepharose 4B column (Amersham Biosciences). Bound proteins were eluted with 10 mM reduced glutathione in 50 mM Tris, pH 8.0. Eluted proteins were concentrated and further purified using a Q-Sepharose high performance column. For the GST-CNTFR_BC and GST-gp130_BC peptides, the GST tag was cleaved using PreScission protease (Amersham Biosciences), and the peptides were further purified using a GST-Sepharose 4B affinity column and a gel filtration column. The peptides were concentrated by ultrafiltration, and their concentrations were determined by a Coomassie plus protein assay (Pierce) and SDS-PAGE.

NMR Spectroscopy—Four NMR samples, with an approximate concentration of 1.0 mM, were prepared for the structure determination of the CNTFR BC domain. These were the unlabeled BC domain in 90% H₂O, 10% D₂O, 15 N-labeled BC domain in 90% H₂O, 10% D₂O, two 15 N/ 13 C-labeled samples, one in 99.9% D₂O and one in 90% H₂O, 10% D₂O. All NMR experiments were performed at 25 °C on Varian Inova 500- and 750-MHz NMR spectrometers equipped with 5-mm inverse z-shielded triple resonance 1 H/ 13 C/ 15 N PFG probes. NMR spectra were processed with the nmrPipe software package (28) and analyzed with PIPP² and SPARKY.³ Complete 1 H, 13 C, and 15 N resonance assignments were obtained as described earlier (15). NOE restraints were derived from a three-dimensional 15 N-NOESY-HSQC experiment (mixing time 200 ms) recorded in H₂O and a three-dimensional 13 C-NOESY-HSQC experiment (mixing time 150 ms) recorded in D₂O. Amide protons in slow exchange with solvent were identified by a series of 1 H- 15 N HSQC experiments on a lyophilized 15 N-labeled sample of the CNTFR BC domain redissolved in D₂O buffer.

15 N longitudinal relaxation times (T_1), 15 N spin-lattice relaxation times (T_2) and 1 H- 15 N NOE measurements (29) were performed at 25 °C on the Varian Inova 500 MHz spectrometer. The relaxation delays, T , for the T_1 experiments are as follows: $T = 0.011, 0.128, 0.267, 0.533, 0.800, 1.120, 1.440, \text{ and } 1.867$ s; and for the T_2 experiments are as follows: $T = 14.1, 28.2, 42.3, 56.4, 70.5, 84.6, 98.7, \text{ and } 112.8$ ms. The recycle delays for the T_1 and T_2 measurements were 2 s. 1 H- 15 N steady-state NOE values were obtained by recording spectra with and without a 3-s 1 H saturation period prior to the start of the experiment. The total recycle delays for the NOE measurements, with and without 1 H saturation, were 4 and 7 s, respectively. A total of 16 transients was recorded in 15 N T_1 and T_2 experiments and 32 in NOE measurements. All spectra were acquired as 512×128 complex data matrices and processed using the nmrPipe software package (28) with peak intensities determined as volumes. The 15 N relaxation rates and uncertainties were determined from nonlinear least squares fitting of the experimental peak intensities to a monoexponential equation with an offset parameter using the program SAS (SAS Institute Inc., Cary, NC). Steady-state NOE values (η) for each of the amide nitrogens were calculated

² D. S. Garrett, spin.niddk.nih.gov/clore/.

³ T. D. Goddard and D. G. Kneller, www.cgl.ucsf.edu/home/sparky/.

from the peak height in the experiment with saturation (I) and that in the reference experiment without saturation (I_0), according to the equation: $\eta = (I - I_0)/I_0$. The T_1 , T_2 relaxation times and NOEs can be expressed in terms of the spectral density function J , which can be modeled using the "model-free" formalism (30, 31). Non-linear least squares fitting and Monte Carlo error analysis were performed using the program Modelfree 4.0 (32, 33).

Unlabeled and ^{15}N -labeled samples of the gp130 BC domain at a concentration of 0.8 mM and a pH of 6.5 were prepared for NMR studies. Sequential assignment for the gp130 BC domain was performed using ^1H - ^{15}N HSQC, ^{15}N -NOESY-HSQC, and ^{15}N -TOCSY-HSQC experiments and with reference to the published assignments (12).

Structure Determination—Distance restraints were calibrated directly from NOESY cross-peak intensities by utilizing the weakest and strongest NOESY cross-peaks (calibrated to 5.0 and 1.8 Å, respectively) to calculate intensity-dependent proportionality factors (34). All lower bound restraints were set to 1.8 Å. Raw ambiguous distance restraint lists were generated from NOESY peak lists by interrogating the chemical shift assignments using windows of 0.03 ppm for proton dimensions and 0.3 ppm for ^{13}C and ^{15}N dimensions in the three-dimensional ^{15}N -NOESY-HSQC and three-dimensional ^{13}C -NOESY-HSQC experiments. Ambiguous restraint lists were iteratively filtered against current coordinate ensembles using the ARIA method (35) to generate unambiguous and ambiguous distance restraint lists. The final restraint statistics are listed in Table I. Hydrogen bond distance restraints were included where amide protons were still visible 12 h after the sample was dissolved in D_2O . The hydrogen-acceptor distance was restrained between 1.5 and 2.4 Å, and the donor-acceptor distance was restrained between 2.5 and 3.4 Å. Values for $^3J_{\text{N}\alpha}$ were estimated from HNHA (36) and nJ-HMQC (37) experiments. Torsion angle restraints for Φ angles of $-120^\circ (\pm 50)$ were imposed for $^3J_{\text{N}\alpha} \geq 8$ Hz and $-60^\circ (\pm 30)$ for $^3J_{\text{N}\alpha} \leq 6$ Hz. Structures were calculated using the simulated annealing protocol included in the ARIA package compiled with the CNS program (38). An ensemble of the lowest 20 energy structures was retained.

ELISA Screening for CNTFR Binding Partners—For screening the binding capability of the individual domains of gp130 and gp130 and LIFR mutants with CNTFR, purified His-sCNTFR-myc, or wild type or mutant CNTFR BC domains were coated on IMMULON®2 (Dynatech) ELISA plates at 10 $\mu\text{g}/\text{ml}$. Nonspecific binding was blocked with PBS containing 0.25% BSA. For the binding partner test, 10 μg of the supernatants of IPTG-induced bacterial lysates after sonication were added to the wells. To test the binding capability of different mutants of the gp130 CBD and LIFR CBD1, purified peptides with serial dilutions in PBS, 0.2 $\mu\text{g}/\mu\text{l}$ BSA were applied. After incubation and washing, bound proteins were detected using a goat anti-gp130 or anti-LIFR antibody (R & D Systems) at 1:2000 dilutions followed by horseradish peroxidase-conjugated secondary antibodies with the same dilutions. To assess the ability of the CNTFR BC domain and its mutants to interact with the gp130 BC domain, equal amounts of the purified GST-BC domain of gp130 (100 $\mu\text{g}/\text{ml}$) in PBS were applied. After incubation and washing, bound proteins were detected with GST antibodies at 1:10,000 dilutions followed by horseradish peroxidase-conjugated secondary antibodies at 1:4000 dilutions. Peroxidase activity was detected by o-phenylenediamine substrate, and the orange colored product was read at 490 nm using an MR5000 microplate reader (Dynatech).

Immunoprecipitation, GST Pull-down Assay, and Western Blotting—Two hundred ng of purified gp130 CBD was incubated with 200 ng of purified His-sCNTFR-myc, 1 μg of anti-Myc antibody, and 10 μg of BSA in 200 μl of PBS overnight at 4 $^\circ\text{C}$. Ten μl of κ -lock (Zymed Laboratories Inc.) beads were then added and incubated for 2 h. Purified GST fusion peptides were incubated with purified His-sCNTFR-myc with serial dilutions in 200 μl of PBS with 20 μg of BSA and 10 μl of glutathione-conjugated Sepharose 4B beads overnight at 4 $^\circ\text{C}$. In both cases, beads were washed with PBS, and 20 μl of 2 \times sample buffer for SDS-PAGE was added. The boiled supernatants were collected, separated by SDS-PAGE, and blotted onto nitrocellulose membranes. After blocking in TBST containing 5% milk powder, membranes were incubated with antibodies (1:1000) specific for CNTFR, gp130, or LIFR at 4 $^\circ\text{C}$ overnight. Membranes were incubated with horseradish peroxidase-conjugated secondary antibodies with 1:2000 dilutions for 1 h at room temperature after washing with TBST. Proteins were detected by chemiluminescence using an ECL kit (Amersham Biosciences) following the manufacturer's instructions.

Alanine Scanning and Site-directed Mutagenesis—Standard PCR-based site-directed mutagenesis procedures were performed for the alanine scanning of the AB loop and B strand in the BC module of the gp130 CBD and the LIFR CBD1 and the mutagenesis of the CNTFR BC

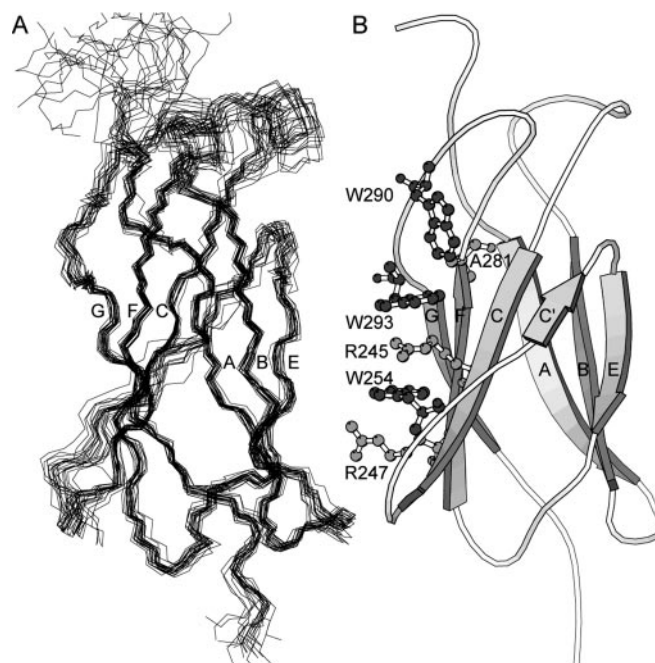


FIG. 2. Structure of the CNTFR BC domain. A, the ensemble of the lowest 20 energy structures. Each structure was superimposed on the energy-minimized average structure using the backbone atoms of the β -strands except for the C' strand. Model 5 is the most representative as defined by NMRCLUST (46). B, ribbon diagram (47), in the same orientation, of the energy-minimized average structure showing the tryptophan-arginine zipper network. In both A and B, the N terminus is at the top of the figure and the C terminus is at the bottom, and the strands are labeled.

domain. gp130 is numbered from the mature peptide, although LIFR and CNTFR are numbered from the signal peptide. The gp130 CBD mutants with amino acids substituted by alanine are as follows: S211A/E212A, E213A/L214A, S215A/S216A, I217A/L218A, K219A/L220A, T221A/W222A, K219A, and L220A. The LIFR CBD1 mutants with alanine substitutions are as follows: D147A/F148A, S149A/T150A, S151A/T152A, L153A/Y154A, and L155A/K156A. CNTFR mutants with alanine substitution of Glu²²³, Thr²²⁵, His²⁵⁶, Glu²⁵⁸, Thr²⁶³, Thr²⁶⁶, Thr²⁶⁸, Thr²⁶⁹, Glu²⁸⁶, and Thr²⁶⁸/Asp²⁶⁹ were constructed. Other CNTFR mutants were E223K, H256E, H256E/E258A, D284K, E286H, E286K, and D284K/E286K. The DNA sequences of all the mutant constructs were verified using an ABI PRISM 310 Genetic Analyzer. All mutants were subsequently expressed as His tag or GST fusion proteins and purified as described above when necessary.

RESULTS

Structure Determination and Backbone Dynamics—The three-dimensional structure of the BC domain of the CNTF α -receptor in aqueous solution at pH 6.5 and 25 $^\circ\text{C}$ was determined by NMR methods. Data were recorded on unlabeled, ^{15}N -labeled, and $^{15}\text{N}/^{13}\text{C}$ -labeled samples, and the chemical shift assignments of the CNTFR BC domain are described elsewhere (15). Following identification of the global-fold from manual inspection of the nuclear Overhauser effect spectroscopy (NOESY) data, ambiguous NOE restraints were resolved using the iterative ARIA method (35), and the structure was determined by simulated annealing using the CNS package (38). The final ensemble of the lowest 20 energy structures of the CNTFR BC domain is shown in Fig. 2A, and in Fig. 2B a ribbon diagram representation of the average structure, in the same orientation, shows the fibronectin type III domain-like topology of seven β -strands in two anti-parallel β -sheets formed by these domains. The first β -sheet consists of three strands: A (Glu²⁰⁸-Pro²¹⁴), B (Leu²²²-Gln²²⁷), and E (Ala²⁶⁴-Ile²⁶⁷), and the second β -sheet is composed of four strands: C (Lys²⁴¹-Pro²⁴⁸), C' (Val²⁵⁷-Leu²⁵⁹), F (Tyr²⁷⁶-Lys²⁸³), and G (Val²⁹⁵-Ala²⁹⁹).

TABLE I
 Structural statistics

| | |
|---|---------------------|
| A. Restraints for structure calculation | |
| Total unambiguous restraints | 1925 |
| Intraresidue | 843 |
| Sequential | 446 |
| Medium range | 131 |
| Long range | 505 |
| Total ambiguous restraints | 575 |
| Hydrogen bond restraints | 33 |
| Dihedral ϕ angle restraints | 63 |
| B. Ensemble r.m.s. deviations from ideal values | |
| Bonds (\AA) ($\times 10^{-3}$) | 3.60 (± 0.07) |
| Angles (degree) | 0.44 (± 0.02) |
| Improper dihedral angles (degree) | 1.48 (± 0.08) |
| C. Coordinate precision | |
| r.m.s.d. of N, C α , and C' atoms | |
| Well defined residues (\AA) | 0.37 (± 0.04) |
| All residues (\AA) | 1.40 (± 0.31) |
| r.m.s.d. of heavy atoms | |
| Well defined residues (\AA) | 0.84 (± 0.23) |
| All residues (\AA) | 1.56 (± 0.23) |
| D. Ramachandran properties (non-Pro/Gly) | |
| Most favored | 1349 (74.9%) |
| Additional allowed | 428 (23.8%) |
| Generously allowed | 16 (0.9%) |
| Disallowed | 7 (0.4%) |

The WSXWS sequence that is characteristic of the class I cytokine receptors (11) is located in the C-terminal part of the FG loop (Trp²⁹⁰-Ser²⁹⁴ in the CNTFR BC domain) and runs roughly antiparallel to the F strand (Fig. 2B). In many of the class I cytokine receptors a third tryptophan (Trp²⁵⁴ in CNTFR) extends the WSXWS motif, forming a ladder of parallel tryptophan side chains. Charged or polar residues from the F and C strands are inserted between the tryptophan residues, forming a charged band on the surface of the domain. In the majority of these receptors a highly conserved arginine residue occupies the space between the side chains of the tryptophans of the WSXWS motif. In the cases of CNTFR and IL-11R, this arginine residue is replaced by alanine (Ala²⁸¹) and serine, respectively. As a consequence the side chain of Trp²⁹⁰ in CNTFR is not parallel to the other tryptophan residues but roughly perpendicular to them, occupying the space where the arginine side chain is found in other receptors and interacting with Phe²⁴³.

The number of restraints used in the structure determination and the structural statistics are summarized in Table I. The ensemble of structures (Fig. 2A) were superimposed using the residues in the β -sheet elements (except the C' strand), and the r.m.s.d. of the ensemble N, C α , and C' atoms of the residues from the mean coordinates are given in Fig. 3A. For the well defined residues (those with r.m.s.d. values within 2σ of the mean value in the global superposition of the ensemble) the r.m.s.d. of the N, C α , and C' atoms from those of the average structure was 0.37 ± 0.04 \AA . Fig. 3B shows the numbers of inter-residue NOEs per residue that were used in the structure calculation. Of the 20 low energy structures in the ensemble, 7 had no residues in the generously allowed or disallowed regions (39) of the Ramachandran plot, and the maximum number of residues in these regions in any one structure was 3.

The backbone dynamics of the BC domain of CNTFR were studied by measuring the ¹⁵N, T₁, and T₂ relaxation times and the ¹H-¹⁵N steady-state NOE values at 25 °C on the Varian Inova 500 MHz spectrometer. Results from the model-free analysis (30–33) showing the generalized order parameters (S²) and the ¹H-¹⁵N steady-state NOE values are presented in Fig. 3 (C and D), respectively. The S² values correspond well to the secondary structure of the protein, with average S² values of 0.90 ± 0.06 and 0.79 ± 0.20 for the sheet and the loop

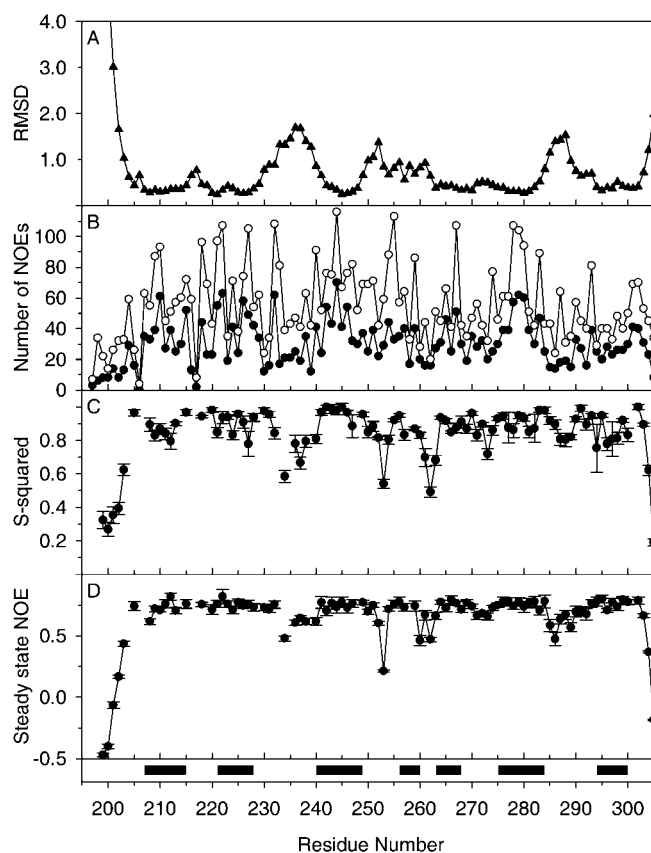


FIG. 3. Structural and dynamics parameters for the CNTFR BC domain. A, average N, C α , and C' atom r.m.s.d. values from the mean coordinates for the ensemble. B, ●, the number of unambiguous and ambiguous inter-residue NOE restraints; ○, the total of NOE restraints for each residue. C, the generalized order parameter S². D, the ¹H-¹⁵N steady-state NOE values for the residues. The locations of the β -strands are shown at the bottom of the figure.

regions, respectively. In particular, the loops between the B-C, C-C', and C'-E strands are very flexible.

Identification of Modules in the Extracellular Region of gp130 That Bind to sCNTFR—To assess the binding capacity of sCNTFR for the domains within the extracellular part of gp130, an ELISA was used. sCNTFR was expressed in bacteria with a polyhistidine tag at the N terminus for ease of purification. Purified His-sCNTFR-myc retained the capacity to bind to purified His-CNTF (data not shown). Purified His-sCNTFR-myc (10 $\mu\text{g/ml}$) was directly coated onto an ELISA plate and as low as 0.025 $\mu\text{g/ml}$ CNTF could be detected using this system (26). We screened for the putative binding modules within the extracellular domain of gp130 using sCNTFR. The individual domain constructs were the Ig, CBD, and Ig-CBD modules of gp130. These domains were expressed as N-terminal His-tagged peptides in *E. coli*. After IPTG induction followed by sonication, supernatants of bacterial lysates with equal amounts of total protein were subjected to Western blotting and ELISA assays. Whereas the CBD and Ig-CBD of gp130 could be detected by Western blot in both the supernatants and pellets after sonication, the Ig-like module of gp130 could only be detected in the pellets (data not shown). We therefore used a fusion protein, GST-Ig of gp130, for the screening. ELISA screening showed that the CBD and Ig-CBD of gp130 could bind with sCNTFR (Fig. 4A). No obvious binding could be detected for the GST-Ig protein. These results indicate that the CBD of gp130 was responsible for the interaction with sCNTFR.

In Vitro Binding of sCNTFR with CBD of gp130—To confirm

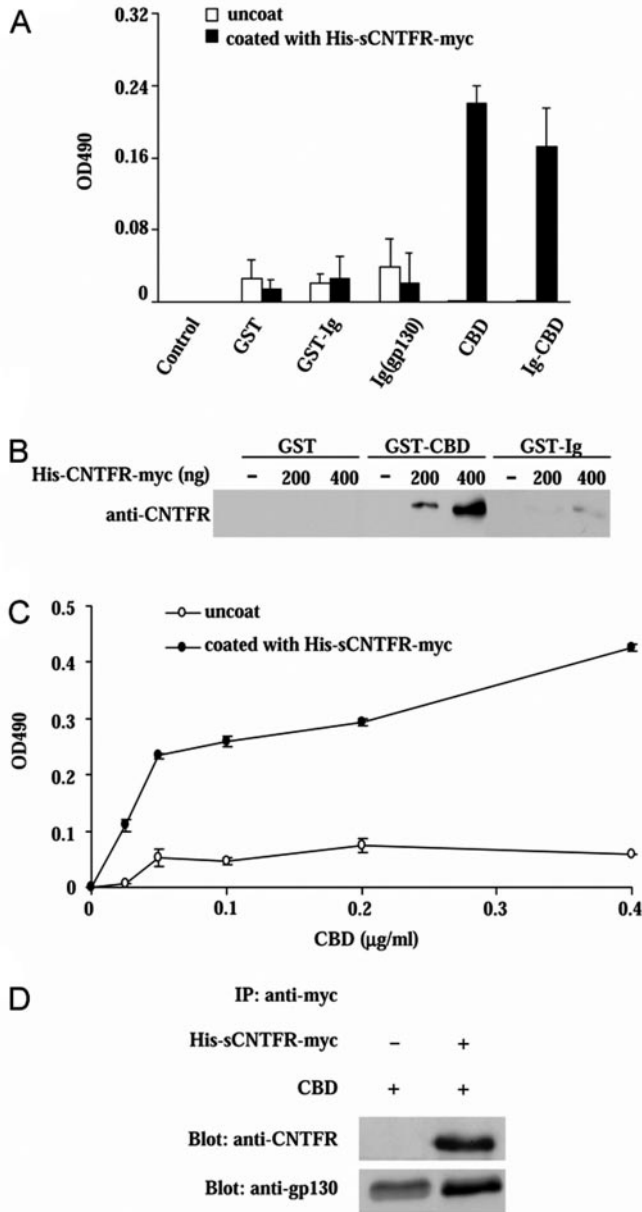


FIG. 4. *In vitro* binding of the CBD of gp130 with His-sCNTFR. A, of the peptides in supernatants of cell lysates only the CBD and Ig-CBD of gp130 bound strongly to His-sCNTFR-myc-coated plates. Results shown represent the mean \pm S.D., $n = 3$. B, the gp130 CBD but not the gp130 Ig domain, as purified GST fusion peptides, could pull-down sCNTFR. C, dose-dependent binding of the His-gp130 CBD to a His-sCNTFR-myc-coated ELISA plate. Results shown represent the mean \pm S.D. of a typical experiment, $n = 4$. D, His-sCNTFR-myc could bind to the His-tagged gp130 CBD as shown by immunoprecipitation (IP) with an anti-Myc antibody.

further the binding capacity of sCNTFR with the CBD of gp130, we performed an *in vitro* pull-down assay. Both the gp130 CBD and the gp130 Ig domain were expressed as GST fusion proteins and purified as described under "Experimental Procedures." Whereas both GST-Ig and GST-CBD fusion proteins could bind to oncostatin M as expected (40) (data not shown), sCNTFR could only be significantly pulled down by the GST-CBD protein and not by the GST-Ig protein (Fig. 4B). The gp130 CBD was also purified as a His-tagged peptide and tested for binding to sCNTFR. As little as 0.025 $\mu\text{g/ml}$ of gp130 CBD could be detected using ELISA (Fig. 4C), a sensitivity comparable with that of CNTF binding to CNTFR. The gp130 CBD could also be pulled down by His-sCNTFR-myc with an anti-Myc antibody (Fig. 4D).

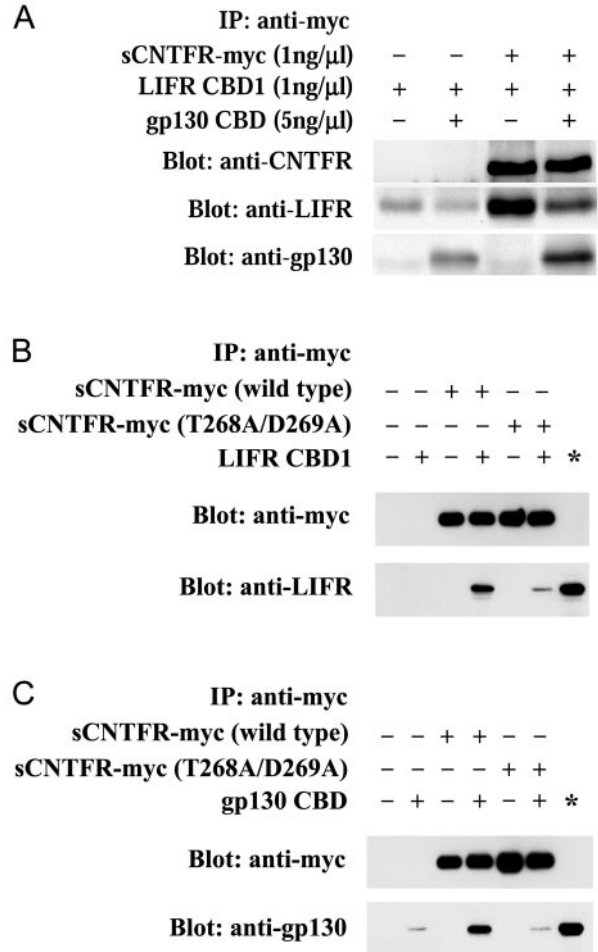


FIG. 5. Competition between the binding of the gp130 CBD and the LIFR CBD1 to sCNTFR-myc. A, binding of the LIFR CBD1 (1 ng/ μl) to sCNTFR-myc (1 ng/ μl) in the presence or absence of a 5-fold excess of gp130 CBD (5 ng/ μl). Overloading of the gp130 CBD inhibited the binding of the LIFR CBD1 with sCNTFR-myc, as shown by immunoprecipitation with an anti-Myc antibody followed by blotting with antibodies specific for CNTFR, LIFR, and gp130. Similar results were obtained from three independent experiments. B and C, *in vitro* interaction of sCNTFR (T268A/D269A) with LIFR CBD1 (B) or the gp130 CBD (C). 200 ng of purified sCNTFR-myc (wild type) or sCNTFR-myc (T268A/D269A) was incubated with or without 200 ng of LIFR CBD1 (B) or gp130 CBD (C) and 1 μg of anti-Myc antibody. The lane marked * indicates the input of LIFR CBD1 (B) or gp130 CBD (C). sCNTFR-myc (T268A/D269A) could only weakly pull down the LIFR CBD1 (B) and could not bind to gp130 CBD (C) as revealed by immunoprecipitation (IP) followed by Western blot using an anti-LIFR antibody.

Competition for the Binding of sCNTFR between LIFR CBD1 and gp130 CBD—We performed a competition assay to test whether the LIFR CBD1 and the gp130 CBD used similar or different binding sites to associate with sCNTFR. Whereas LIFR CBD1 (1 ng/ μl) could bind to sCNTFR (1 ng/ μl) as reported previously (26), a 5-fold excess of gp130 CBD (5 ng/ μl) was found to inhibit this binding (Fig. 5A). A CNTFR mutant with alanine substitution of Thr²⁶⁸/Asp²⁶⁹ (41) could weakly bind to the LIFR CBD1 (Fig. 5B) and lost the capacity to bind to the gp130 CBD (Fig. 5C).

Alanine Scanning Mutagenesis of the AB Loop and B Strand in the BC Module of the gp130 CBD—Residues located in the AB loop and B strand of the BC module of the gp130 CBD, as defined by the crystal structures (13, 14), were mutated to alanine. A series of double mutations covering this region were constructed and expressed as N-terminal His-tagged peptides in *E. coli*. After IPTG induction followed by sonication, supernatants of bacterial lysates with equal amounts of total protein

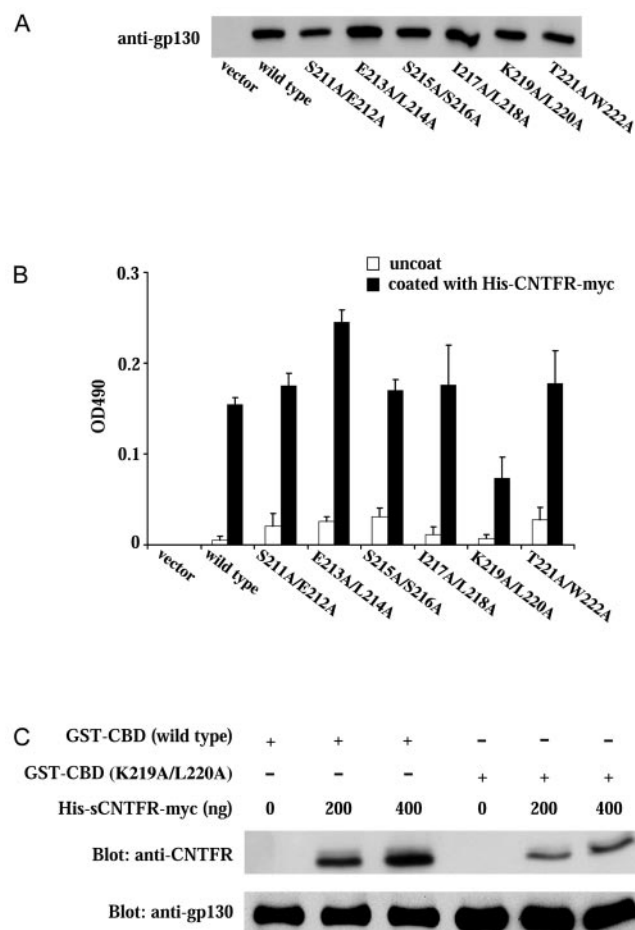


FIG. 6. Alanine scanning of the AB loop and B strand in the BC module of the gp130 CBD. gp130 CBD mutants were expressed as His-tagged peptides in *E. coli* cells. **A**, SDS-PAGE followed by Western blot analysis of the lysate supernatants using an anti-gp130 antibody. **B**, only the gp130 CBD mutant K219A/L220A showed reduced binding capability to sCNTFR (by ~50%) as assayed using ELISA. Results shown represent the mean \pm S.D., $n = 3$. **C**, the gp130 CBD (K219A/L220A) and wild type gp130 CBD were further purified as GST fusion proteins. An *in vitro* pull-down assay showed that the binding of purified His-sCNTFR-myc to the mutant was reduced when compared with that of wild type.

were subjected to Western blotting and ELISAs. Although the total amount of the gp130 CBD mutants and wild type in the supernatant was similar (Fig. 6A), the binding of the K219A/L220A mutant to sCNTFR was reduced by ~50% when compared with other mutants and the wild type gp130 CBD (Fig. 6B). The K219A/L220A mutant was also purified as a GST fusion protein to test its binding capacity with sCNTFR by an *in vitro* pull-down assay. GST-gp130 CBD (K219A/L220A) partially lost its ability to bind to sCNTFR when compared with GST-gp130 CBD (Fig. 6C).

In Vitro Binding of gp130 CBD (K219A) and gp130 CBD (L220A) with sCNTFR—To define the individual contribution of Lys²¹⁹ and Leu²²⁰ to the binding of the gp130 CBD to sCNTFR, we constructed gp130 CBD peptides with single alanine mutations of Lys²¹⁹ and Leu²²⁰. The gp130 CBD(K219A), gp130 CBD(L220A), and wild type gp130 CBD were purified as His-tagged peptides (Fig. 7A). Far-UV circular dichroism spectra of these peptides were similar (data not shown), suggesting that the mutations of Lys²¹⁹ and Leu²²⁰ did not dramatically change the overall secondary structure of the proteins. An ELISA showed that binding of the two mutants to sCNTFR was reduced when compared with that of the wild type gp130 CBD,

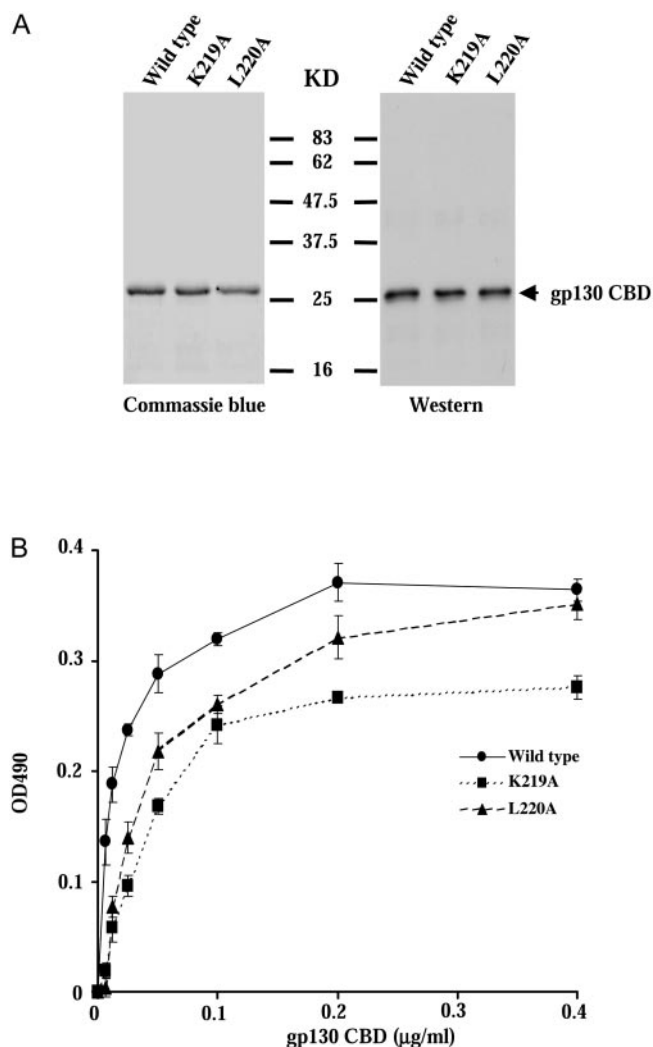


FIG. 7. In vitro binding of gp130 CBD (K219A) and gp130 CBD (L220A) with sCNTFR. **A**, wild type gp130 CBD, gp130 CBD (K219A), and gp130 CBD (L220A) were purified as His-tagged peptides to more than 95% homogeneity as shown by SDS-PAGE followed by Coomassie Blue staining and Western blotting using polyclonal anti-gp130 antibodies. **B**, the binding capacity of the gp130 CBD mutants to sCNTFR was reduced when compared with that of wild type CBD, as revealed by an ELISA. Results shown represent the mean \pm S.D., $n = 3$.

and the binding capacity of gp130 CBD (K219A) was weaker than that of gp130 CBD (L220A) (Fig. 7B).

Alanine Scanning Mutagenesis of the Putative AB Loop and B Strand in the BC Module of the LIFR CBD1—We reported previously (26) that the LIFR CBD1 could interact with sCNTFR *in vitro*. As the gp130 CBD could compete with the LIFR CBD1 for the binding of sCNTFR, we tried to address whether similar amino acids within the putative B strand of the LIFR CBD1 BC module could also be involved in the CNTFR binding. We constructed LIFR CBD1 mutants with double alanine substitutions of residues in the putative B strand of the BC module. LIFR CBD1 mutants were expressed as N-terminal His-tagged peptides in *E. coli*. After IPTG induction followed by sonication, supernatants of bacterial lysates with equal amounts of total protein were subjected to Western blotting and ELISAs. Whereas the total amount of LIFR CBD1 mutants and wild type in the supernatant was similar except for that of LIFR CBD1 (D147A/F148A) (Fig. 8A), the binding of the LIFR CBD1 mutants to sCNTFR was reduced when compared with that of the wild type LIFR CBD1 (Fig. 8B). Interestingly, alanine substitution of amino acids Leu¹⁵⁵/Lys¹⁵⁶ in LIFR CBD1,

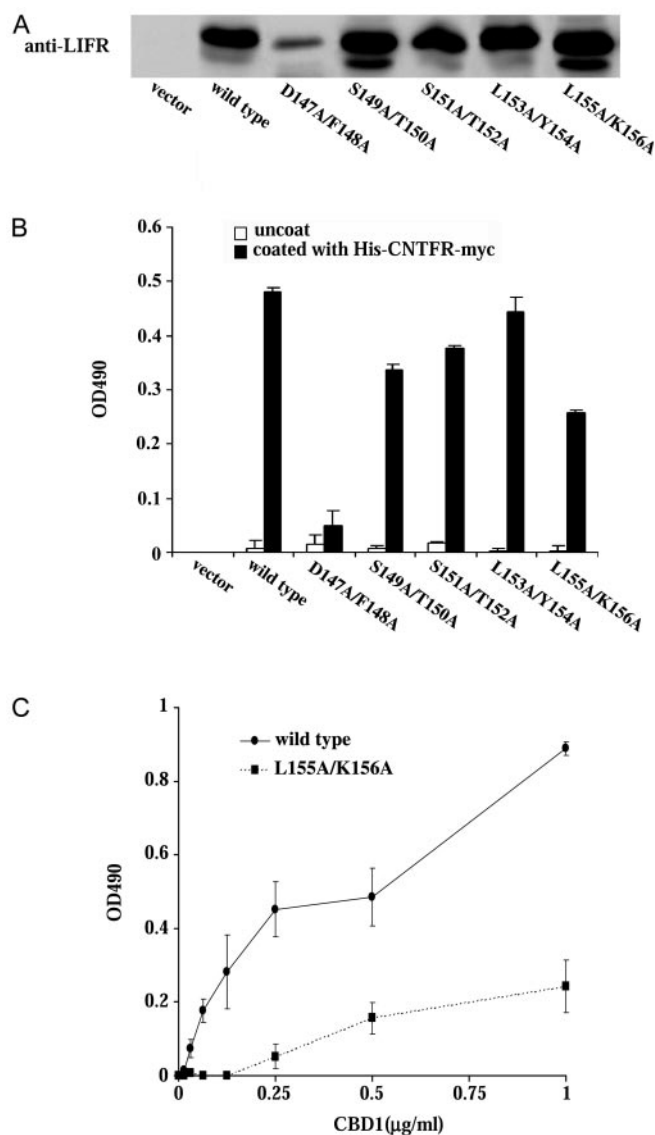


FIG. 8. Alanine scanning of the putative AB loop and B strand in the BC module of the LIFR CBD1. LIFR CBD1 mutants were expressed as His-tagged peptides in *E. coli* cells. *A*, SDS-PAGE followed by Western blot analysis of lysate supernatants using an anti-LIFR antibody. The expression of the D147A/F148A mutant is much lower when compared with that of other mutants and wild type CBD1. *B*, LIFR CBD1 mutants showed reduced binding capability to sCNTFR as assayed using ELISA. Results shown represent the mean \pm S.D., $n = 3$. *C*, the binding capacity of purified LIFR CBD1 (L155A/K156A) to sCNTFR was reduced when compared with that of purified wild type LIFR CBD1, as revealed by an ELISA. Results shown represent the mean \pm S.D., $n = 3$.

which locate at the putatively similar region as that of Lys²¹⁹/Leu²²⁰ in gp130 CBD, reduced the binding of CBD1 to sCNTFR by \sim 50%. Therefore, the L155A/K156A mutant was selected for further study. An ELISA showed that binding of the purified L155A/K156A mutant to sCNTFR was significantly reduced when compared with that of the wild type LIFR CBD1 (Fig. 8C).

Mutagenesis of the CNTFR BC Domain—Several single and double point mutants of the CNTFR BC domain were constructed, and the purified mutant proteins were directly coated onto ELISA plates. Equal amounts of the gp130 BC domain were then added to the plate. Apart from the H256A, T266A, and E286A mutants, which showed slightly increased binding to gp130, the CNTFR BC domain mutants showed slight to moderate reductions in binding capacity (Fig. 9). Alanine mu-

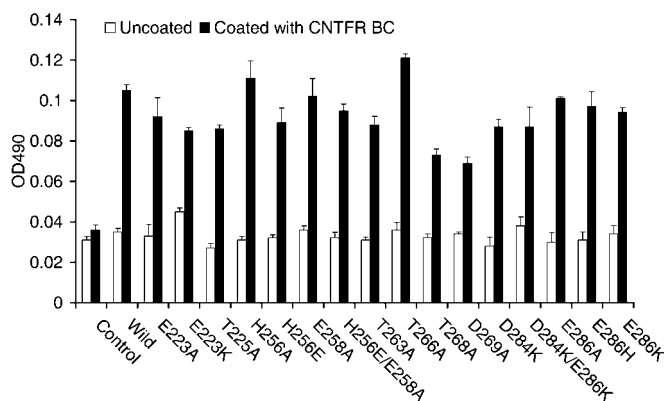


FIG. 9. Mutagenesis of residues in the BC domain of CNTFR. The effect on the binding of gp130 by the CNTFR BC domain mutants as assayed using ELISA. Relative changes reported in the text were calculated as the ratio of the (coated-uncoated) values for the mutant to that of wild type. Results shown represent the mean \pm S.D., $n = 3$.

tations of Thr²⁶⁸ and Asp²⁶⁹ at the N-terminal end of the E-F loop showed the greatest effect (a reduction of 40–50%) on the binding of the gp130 BC domain, consistent with the finding above and earlier results (41) for the CNTFR CBD double mutant of these residues. The charge reversal mutation E223K in the B strand of the CNTFR BC domain reduced binding by about 40%, whereas the alanine mutations of Glu²²³ and Thr²²⁵ had an effect of about 15%. Charge reversals in other parts of the molecule, H256E near the C' loop and D284K and E286K in the F-G loop also reduced binding by around 15% with the double charge reversal of Asp²⁸⁴ and Glu²⁸⁶ having a roughly additive effect.

NMR Study of the Interaction between the BC Domains of CNTFR and gp130—Based on the biochemical studies of the interaction between CNTFR and gp130, a structural study of the interaction surface between the BC domains was undertaken. Titrations of the ¹⁵N-labeled CNTFR BC domain with the unlabeled gp130 BC domain, as well as the inverse titration of the ¹⁵N-labeled gp130 BC domain with the unlabeled CNTFR BC domain were performed. Fig. 10 shows the normalized chemical shift changes of each residue on the CNTFR and gp130 BC domains after the titrations. Several residues showed significant chemical shift perturbations (>0.04 ppm for CNTFR BC and >0.023 ppm for gp130 BC) of their NMR signals after binding.

DISCUSSION

CNTF and its specific receptor, CNTFR, are increasing in importance due to the recent findings that CNTF may have a significant role in the treatment of obesity and diabetes (6), demyelinating central nervous system disease (7), and the identification of cardiotrophin-like cytokine/cytokine-like factor-1 as the long hypothesized second ligand for CNTFR (42). Unlike IL-6 and IL-11, CNTF has an asymmetric signaling complex, involving gp130 and LIFR, and so must contain some receptor-receptor interactions different from those seen in the IL-6 complex (14, 21). A detailed understanding of the CNTF receptor complex will help in developing CNTF and cardiotrophin-like cytokine/cytokine-like factor-1 as potential therapeutic agents.

To provide more insights into the protein-protein interactions in the CNTF receptor complex, we undertook a strategy determining the three-dimensional structure of the BC module of CNTFR as this is the domain that is expected to be involved in receptor-receptor interactions. This was followed by determining which domains in gp130 interacted with CNTFR and a mutagenesis analysis to identify which residues in CNTFR,

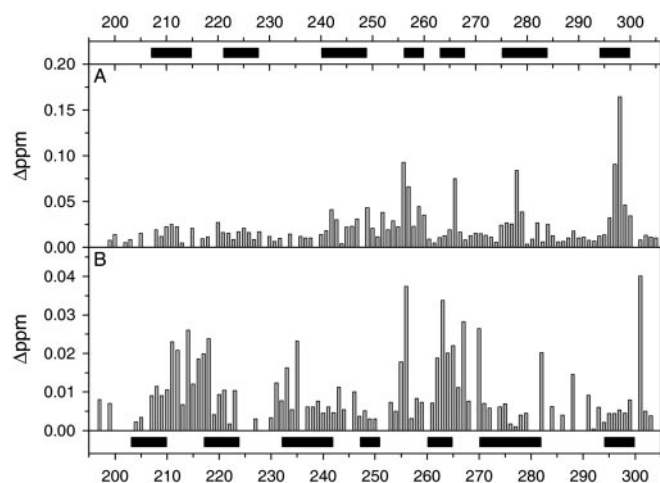


FIG. 10. **Chemical shift perturbation upon binding between CNTFR and gp130 BC domains.** Normalized chemical shift differences ($= ((\text{chemical shift difference in } ^1\text{H})^2 + (\text{chemical shift difference in } ^{15}\text{N}/6)^2)^{1/2}$) of ^{15}N and ^1H amide resonances for the CNTFR BC domain after binding with the gp130 BC domain (A) and the gp130 BC domain after binding with the CNTFR BC domain (B). The secondary structure of each molecule is also indicated.

LIFR, and gp130 might affect receptor interactions. Finally, an NMR study of the chemical shift changes when the CNTFR and gp130 BC domains interact was used to map further the interaction surface. The CNTFR BC domain structure assists in the explanation of these data.

The CNTFR BC domain formed a 7-stranded β -sandwich structure with the Greek key topology characteristic of fibronectin type III domains and the class 1 cytokine receptors. An extended "WSXWS" motif, similar to that seen in the growth hormone receptor (43), was formed in the structure with Arg²⁴⁵ and Arg²⁴⁷ in the C strand, Trp²⁵⁴ near the C' strand, and Ile²⁷⁷ and Gln²⁷⁹ of the F strand completing the extension of the motif. This extension is seen in many but not all of the class 1 cytokine receptors and is the most variable part of this generally conserved region. CNTFR and IL-11R are unusual among these receptors as they do not have an arginine residue intercalating between the two tryptophan residues of the WSXWS motif. At the corresponding position in CNTFR (residue 281), there is an alanine, and in the similar IL-11R sequence a serine is found in this position. A phylogenetic analysis of the gp130 family receptor BC domains (data not shown) shows that the non-signaling receptors form a clade and CNTFR and IL-11R are more similar to each other than to IL-6R. The ability of the usually conserved arginine to be replaced by a small residue such as alanine or serine, altering the structure of the tryptophan ladder usually found in these receptors, might be associated with the fact that these receptors cannot transduce a signal.

Thr²⁶⁸ and Asp²⁶⁹ were earlier identified (41) as important for the interaction of CNTFR with gp130. These residues are located immediately C-terminal to the E strand of the CNTFR BC domain and interact with Arg²²⁰ and Arg²²¹ at the N terminus of the B strand, stabilizing this region of the structure. From the NMR dynamics study, it was shown that the CNTFR BC domain is a very stable structure, with regions of higher mobility in the BC, CC', and C' E loops. Structural flexibility correlated well with the ensemble r.m.s.d. values.

For the study of gp130, once the correct folding of the gp130 peptides was confirmed and the influence of GST on the results was ruled out, it was found that only gp130 peptides containing the CBD could interact with CNTFR in the absence of CNTF. We recently reported that the LIFR CBD1 could interact *in vitro* with CNTFR in the absence of CNTF (26). Due to the

similar effects observed with both of the soluble CBDs, we asked whether these domains were interacting with the same site on CNTFR and therefore whether they would compete with each other for CNTFR binding. Indeed, it was found that a 5-fold excess of the gp130 CBD would inhibit the binding of the LIFR CBD1, consistent with the possibility that they are utilizing similar sites on CNTFR. Here we found that a CNTFR mutant with alanine substitution of Thr²⁶⁸/Asp²⁶⁹, the residues found earlier to be important for CNTFR interaction with other receptors (41), could bind to the LIFR CBD1 much more weakly when compared with the binding of wild type CNTFR and that this mutant CNTFR had lost the capacity to bind to the gp130 CBD. These data suggest that the LIFR CBD1 and the gp130 CBD bind in a very similar manner to the CNTFR.

Our findings provide strong evidence that both CBDs interact with CNTFR in the manner of a β -receptor binding to the α -receptor as seen for the growth hormone receptors (43) and has implications for the nature of the signaling CNTF receptor complex. To test whether the soluble CBDs were interacting with CNTFR in this manner, site-directed mutagenesis studies were undertaken. Based on the crystal structure of growth hormone and its receptors (43) and site-directed mutagenesis studies on CNTFR (41) and IL-6R (44), residues in the AB loop, B and E strands of the BC modules of the gp130 CBD and the LIFR CBD1 might be expected to be involved in CNTFR-gp130 and CNTFR-LIFR interactions, respectively.

Two residues, Lys²¹⁹ and Leu²²⁰ in the putative B strand of the BC module of the gp130 CBD, when mutated to Ala, were found to affect the ligand-free association of mutant gp130 CBD with CNTFR. This was the case for the double mutant and both point mutants. Far UV circular dichroism spectra of the point mutants showed that this effect was not due to gross destabilization of the structure of the gp130 CBD. As Leu²²⁰ is in the hydrophobic core of the BC module, as shown by the crystal structures (13, 14), its effect must be caused by local destabilization of the binding region. Lys²¹⁹, however, is solvent-exposed in the region of gp130 that is expected to interact with the cytokine-specific receptors and had a greater effect on the ability of the gp130 CBD to bind CNTFR (Fig. 11A).

A similar mutagenesis strategy was applied to the LIFR CBD1. Mutation of residues in the putative B strand of the LIFR CBD1 BC module indeed led to reduced binding of these mutants to CNTFR. Based on a homology model of this domain (45), Lys¹⁵⁶ is solvent-exposed in a similar structural position to Lys²¹⁹ of gp130 (Fig. 11A). Indeed, alanine substitution of Leu¹⁵⁵ and Lys¹⁵⁶ reduced the binding of the LIFR CBD1 to CNTFR more significantly than that of other CBD1 mutants. As mutation of these residues in both molecules reduced, but did not abolish, CNTFR binding, other residues might also be involved in these interactions. However, the position of these residues provides further evidence that the ligand-free interaction of CNTFR with both the gp130 CBD and the LIFR CBD1 is the same for both molecules and a similar interaction to that seen between the growth hormone receptors (43).

Mutagenesis of the CNTFR BC domain also revealed residues that affected the interaction with the gp130 BC domain. The greatest effect was observed with the individual mutation of residues Thr²⁶⁸ and Asp²⁶⁹, which showed a decrease in binding of >40%. This matches the earlier finding of others (41) and the effect of the double mutant of these residues noted above. Whereas most of the other mutations generally had more modest effects on the interaction with the gp130 BC domain, the charge reversal mutation E223K also decreased the interaction by about 40%. This residue is in the B strand of the CNTFR BC domain (Fig. 11A). Alanine substitution of Glu²²³ and also that of Thr²²⁵ had a lesser effect (about 15%),

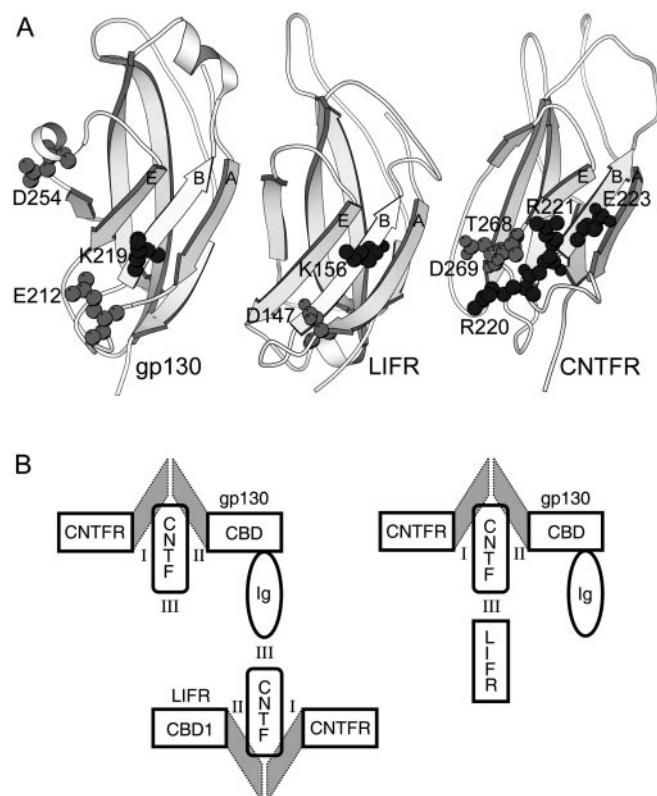


FIG. 11. Residues affecting receptor-receptor interactions and receptor complex models. *A*, ribbon diagrams (47) showing the residues in the region of the A, B, and E β -strands of the BC domains of the gp130 CBD, the LIFR CBD1, and the CNTFR CBD that affect receptor binding. The lysine residues in gp130 and LIFR that affect receptor-receptor interactions and the negatively charged residues in gp130 and LIFR that may interact with CNTFR are shown. For CNTFR, mutation of Thr²⁶⁸ and Asp²⁶⁹ was shown here and earlier (41) to affect CNTFR receptor-receptor interactions. Within CNTFR, Asp²⁶⁹ interacts with Arg²²⁰ and Thr²⁶⁸ with Arg²²¹ which also interacts with Glu²²³. Based on superposition on the growth hormone receptor structures (43), Arg²²⁰, Arg²²¹, and Asp²⁶⁹ appear to interact, respectively, with Glu²¹², Asp²⁵⁴, and Lys²¹⁹ of gp130, and Arg²²⁰ and Asp²⁶⁹ appear to interact with Asp¹⁴⁷ and Lys¹⁵⁶, respectively, of LIFR. Mutation of these residues will destabilize the local structure of the molecule and the intermolecular interactions. The N terminus of each molecule is at the top of the figure. *B*, schematic models of the hexameric (16, 19, 45) and tetrameric (24, 25) models of the CNTFR receptor complex. The interaction of the BC domains of the receptors is indicated by the gray parallelograms located below the CNTFR molecule in the figure.

emphasizing the role of the electrostatic interaction in binding. It was due to the similarity of the electrostatic isopotential surfaces of models of the gp130 CBD and the LIFR CBD1 that it was earlier suggested that the LIFR CBD1 might be the partner for CNTFR in the hexameric complex (45). In this complex the BC domains of the LIFR CBD1 and the gp130 CBD would interact with the BC domain of CNTFR through the juxtaposition of the regions of each molecule that contain the A, B, and E strands (Fig. 11).

By superimposing the structure of the BC domain of CNTFR and the structure of gp130 (13, 14) onto that of the growth hormone receptor complex (43), the surfaces of the A, B, and E strands of both molecules interact with each other. It can be seen that Lys²¹⁹ of gp130 is likely to form a salt bridge with Asp²⁶⁹ of CNTFR. Asp²⁶⁹ may also form an intramolecular salt bridge with Arg²²⁰ of CNTFR, which in turn interacts with Glu²¹² of gp130. Asp²⁵⁴ of gp130 is in close proximity to Arg²²¹ of CNTFR which forms a hydrogen bond with Thr²⁶⁸ of CNTFR (Fig. 11A). The lack of these inter- and intramolecular interactions in the T268A/D269A double mutant of CNTFR and the

consequent local structural destabilization of the environment of Arg²²⁰ and Arg²²¹ is consistent with the inability of this mutant to bind the gp130 CBD. Glu²²³ and Arg²²¹ of CNTFR are in close proximity (Fig. 11), and so the charge reversal mutant E223K may displace Arg²²¹ and so affect its interaction with Asp²⁵⁴ of gp130. The other charge reversal mutants that had some effect on binding are close to the WSXWS motif and may destabilize the structure. If the homology model of the LIFR CBD1 (45) is superimposed on the growth hormone receptor structure (43), then Lys¹⁵⁶ of LIFR makes a weaker interaction with Asp²⁶⁹ of CNTFR and Asp¹⁴⁷ of the LIFR CBD1 interacts with Arg²²⁰ of CNTFR. This could explain the residual interaction of the LIFR CBD1 with the T268A/D269A double mutant of CNTFR.

An NMR chemical shift perturbation study of the interaction sites on the CNTFR BC domain and the gp130 BC domain, with each domain labeled alternatively, revealed many residues whose ¹⁵N chemical shifts altered on binding. On gp130 residues in the AB loop and the E strand, which are close to the interaction surface identified by mutagenesis, a significant effect was shown. In the case of the CNTFR BC domain, residue Thr²⁶⁶ in the E strand, which is close to the important binding residues Thr²⁶⁸ and Asp²⁶⁹ and showed an increase in binding affinity when mutated to alanine, had an altered chemical shift. Other residues that were affected were located in the F and G strands of the BC domain and would be expected to be away from the binding surface. The majority of these residues, such as Ile²⁷⁸ in the F strand, were buried in the structure. A limitation of this approach is that, by using HSQC experiments, only the backbone amide nitrogen is monitored. Many of the perturbations observed will not reflect side chain-side chain interactions affected by binding but local structural adjustments to the backbone due to the contact of the two molecules.

Our findings have demonstrated that, *in vitro*, CNTFR and either the gp130 CBD or the LIFR CBD1 can form dimers in the absence of CNTF, and we have identified residues important for these interactions. The location of the critical residues and the ability of the two CBDs to compete with each other for CNTFR binding suggest that this *in vitro* ligand-free interaction may be similar to the *in vivo* binding mode. These data are more consistent with the hexameric model of the CNTF receptor complex, where CNTFR is proposed to interact with both gp130 and LIFR through the same site (16, 19, 45), than the tetrameric model in which LIFR does not necessarily contact CNTFR, but if it did it would not be through the same site as gp130 (24, 25) (Fig. 11B).

Acknowledgment—The Hong Kong Biotechnology Research Institute is acknowledged for the purchase of the 750 MHz NMR spectrometer.

REFERENCES

- Taga, T., and Kishimoto, T. (1997) *Annu. Rev. Immunol.* **15**, 797–819
- Senaldi, G., Varnum, B. C., Sarmiento, U., Starnes, C., Lile, J., Scully, S., Guo, J., Elliott, G., McNinch, J., Shaklee, C. L., Freeman, D., Manu, F., Simonet, W. S., Boone, T., and Chang, M. S. (1999) *Proc. Natl. Acad. Sci. U. S. A.* **96**, 11458–11463
- Shi, Y., Wang, W., Yourey, P. A., Gohari, S., Zukauskas, D., Zhang, J., Ruben, S., and Alderson, R. F. (1999) *Biochem. Biophys. Res. Commun.* **262**, 132–138
- Sleeman, M. W., Anderson, K. D., Lambert, P. D., Yancopoulos, G. D., and Wiegand, S. J. (2000) *Pharm. Acta Helv.* **74**, 265–272
- The ALS CNTF Treatment Study Phase I–II Study Group (1996) *Arch. Neurol.* **53**, 141–147
- Lambert, P. D., Anderson, K. D., Sleeman, M. W., Wong, V., Tan, J., Hijarunguru, A., Corcoran, T. L., Murray, J. D., Thabet, K. E., Yancopoulos, G. D., and Wiegand, S. J. (2001) *Proc. Natl. Acad. Sci. U. S. A.* **98**, 4652–4657
- Linker, R. A., Maurer, M., Gaupp, S., Martini, R., Holtmann, B., Giess, R., Rieckmann, P., Lassmann, H., Toyka, K. V., Sendtner, M., and Gold, R. (2002) *Nat. Med.* **8**, 620–624
- DeChiara, T. M., Vejsada, R., Poueymirou, W. T., Acheson, A., Suri, C., Conover, J. C., Friedman, B., McClain, J., Pan, L., Stahl, N., and Yancopoulos, G. D. (1995) *Cell* **83**, 313–322
- Heinrich, P. C., Behrmann, I., Müller-Newen, G., Schaper, F., and Graeve, L.

- (1998) *Biochem. J.* **334**, 297–314
10. Rane, S. G., and Reddy, E. P. (2000) *Oncogene* **19**, 5662–5679
 11. Bazan, J. (1990) *Proc. Natl. Acad. Sci. U. S. A.* **87**, 6934–6938
 12. Kernebeck, T., Pflanz, S., Müller-Newen, G., Kurapkat, G., Scheek, R. M., Dijkstra, K., Heinrich, P. C., Wollmer, A., Grzesiek, S., and Grötzinger J. (1999) *Protein Sci.* **8**, 5–12
 13. Bravo, J., Staunton, D., Heath, J. K., and Jones, E. Y. (1998) *EMBO J.* **17**, 1665–1674
 14. Chow, D., He, X., Snow, A. L., Rose-John, S., and Garcia, K. C. (2001) *Science* **291**, 2150–2155
 15. Man, D., Xia, Y., Sze, K. H., Smith, D. K., He, W., Ip, N. Y., and Zhu, G. (2002) *J. Biomol. NMR* **22**, 95–96
 16. De Serio, A., Graziani, R., Laufer, R., Ciliberto, G., and Paonessa, G. (1995) *J. Mol. Biol.* **254**, 795–800
 17. Ward, L. D., Howlett, G. J., Discolo, G., Yasukawa, K., Hammacher, A., Moritz, R. L., and Simpson, R. J. (1994) *J. Biol. Chem.* **16**, 23286–23289
 18. Paonessa, G., Graziani, R., De Serio, A., Savino, R., Ciapponi, L., Lahm, A., Salvati, A. L., Toniatti, C., and Ciliberto, G. (1995) *EMBO J.* **14**, 1942–1951
 19. Simpson, R. J., Hammacher, A., Smith, D. K., Matthews, J. M., and Ward, L. D. (1997) *Protein Sci.* **6**, 929–955
 20. Hammacher, A., Richardson, R. T., Layton, J. E., Smith, D. K., Angus, L. J., Hilton, D. J., Nicola, N. A., Wijdenes, J., and Simpson, R. J. (1998) *J. Biol. Chem.* **273**, 22701–22707
 21. Chow, D., Ho, J., Nguyen Pham, T. L., Rose-John, S., and Garcia, K. C. (2001) *Biochemistry* **40**, 7593–7603
 22. McDonald, N. Q., Panayotatos, N., and Hendrickson, W. A. (1995) *EMBO J.* **14**, 2689–2699
 23. Panayotatos, N., Radziejewska, E., Acheson, A., Somogyi, R., Thadani, A., Hendrickson, W. A., and McDonald, N. Q. (1995) *J. Biol. Chem.* **270**, 14007–14014
 24. Kallen, K. J., Grotzinger, J., Lelievre, E., Vollmer, P., Aasland, D., Renne, C., Mullberg, J., Myer zum Buschenfelde, K. H., Gascan, H., and Rose-John, S. (1999) *J. Biol. Chem.* **274**, 11859–118670
 25. Grotzinger, J., Kernebeck, T., Kallen, K. J., and Rose-John, S. (1999) *Biol. Chem.* **380**, 803–813
 26. He, W., Gong, K., Zhu, G., Smith, D. K., and Ip, N. Y. (2002) *FEBS Lett.* **514**, 214–218
 27. Panayotatos, N., Everdeen, D., Liten, A., Somogyi, R., and Acheson, A. (1994) *Biochemistry* **33**, 5813–5818
 28. Delaglio, F., Grzesiek, S., Vuister, G. W., Zhu, G., Pfeifer, J., and Bax, A. (1995) *J. Biomol. NMR* **6**, 277–293
 29. Farrow, N. A., Muhandiram, R., Singer, A. U., Pascal, S. M., Kay, C. M., Gish, G., Shoelson, S. E., Pawson, T., Forman-Kay, J. D., and Kay, L. E. (1994) *Biochemistry* **33**, 5984–6003
 30. Lipari, G., and Szabo, A. (1982) *J. Am. Chem. Soc.* **104**, 4546–4559
 31. Clore, M. G., Szabo, A., Bax, A., Kay, L. E., Driscoll, P. C., and Gronenborn, A. M. (1990) *J. Am. Chem. Soc.* **112**, 4989–4991
 32. Palmer, A. G., Rance, M., and Wright, P. E. (1991) *J. Am. Chem. Soc.* **113**, 4371–4380
 33. Mandel, A. M., Akke, M., and Palmer, A. G. (1995) *J. Mol. Biol.* **246**, 144–163
 34. Xu, R. X., Word, J. M., Davis, D. G., Rink, M. J., Willard, D. H., and Gampe, R. T. (1995) *Biochemistry* **34**, 2107–2121
 35. Nilges, M., Macias, M. M., O'Donoghue, S. I., and Oschkinat, H. (1997) *J. Mol. Biol.* **269**, 408–422
 36. Vuister, G. W., and Bax, A. (1993) *J. Am. Chem. Soc.* **115**, 7772–7777
 37. Xia, Y., Kong, X., Ip, N., and Zhu, G. (2000) *J. Magn. Reson.* **146**, 228–231
 38. Brünger, A. T., Adams, P. D., Clore, G. M., DeLano, W. L., and Gros, P. (1998) *Acta Crystallogr. Sect. D Biol. Crystallogr.* **54**, 905–921
 39. Laskowski, R. A., MacArthur, M. W., Moss, D. S., and Thornton, J. M. (1993) *J. Appl. Crystallogr.* **26**, 283–291
 40. Staunton, D., Hudson, K. R., and Heath, J. K. (1998) *Protein Eng.* **11**, 1093–1102
 41. Auguste, P., Robledo, O., Olivier, C., Froger, J., Praloran, V., Pouplard-Barthelax, A., and Gascan, H. (1996) *J. Biol. Chem.* **271**, 26049–26056
 42. Elson, G. C., Lelievre, E., Guillet, C., Chevalier, S., Plun-Favreau, H., Froger, J., Suard, I., de Coignac, A. B., Delneste, Y., Bonnefoy, J. Y., Gauchat, J. F., and Gascan, H. (2000) *Nat. Neurosci.* **3**, 867–872
 43. de Vos, A. M., Ultsch, M., and Kossiakoff, A. A. (1992) *Science* **255**, 306–312
 44. Salvati, A. L., Lahm, A., Paonessa, G., Ciliberto, G., and Toniatti, C. (1995) *J. Biol. Chem.* **270**, 12242–12249
 45. Smith, D. K., and Treutlein, H. R. (1998) *Protein Sci.* **7**, 886–896
 46. Kelley, L. A., Gardner, S. P., and Sutcliffe, M. J. (1996) *Protein Eng.* **9**, 1063–1065
 47. Kraulis, P. (1991) *J. Appl. Crystallogr.* **24**, 946–950